

# Charge-Asymmetry of the Nucleon-Nucleon Interaction

G. Q. Li\* and R. Machleidt†

*Department of Physics, University of Idaho, Moscow, ID 83844, U.S.A.*

(August 4, 2018)

Based upon the Bonn meson-exchange model for the nucleon-nucleon ( $NN$ ) interaction, we study systematically the charge-symmetry-breaking (CSB) of the  $NN$  interaction due to nucleon mass splitting. Particular attention is paid to CSB generated by the  $2\pi$ -exchange contribution to the  $NN$  interaction,  $\pi\rho$  diagrams, and other multi-meson-exchanges. We calculate the CSB differences in the  $^1S_0$  effective range parameters as well as phase shift differences in  $S$ ,  $P$  and higher partial waves up to 300 MeV lab. energy. We find a total CSB difference in the singlet scattering length of 1.6 fm which explains the empirical value accurately. The corresponding CSB phase-shift differences are appreciable at low energy in the  $^1S_0$  state. In the other partial waves, the CSB splitting of the phase shifts is small and increases with energy, with typical values in the order of 0.1 deg at 300 MeV in  $P$  and  $D$  waves.

arXiv:nucl-th/9804023v1 9 Apr 1998

---

\*Present Address: Department of Physics, SUNY, Stony Brook, NY 11794

†Electronic address: machleid@uidaho.edu

## I. INTRODUCTION

Charge-symmetry is the equality of proton-proton ( $pp$ ) and neutron-neutron ( $nn$ ) forces—after electromagnetic effects are removed. This symmetry, which is slightly broken, has long been a subject of research in nuclear physics (for reviews see, e. g., Refs. [1–4]). Traditionally, the empirical information on the charge-asymmetry of the nuclear force comes mainly from few-body systems. The nucleon-nucleon ( $NN$ ) scattering length in the  $^1S_0$  state plays a special role. As there exists an almost bound state in that partial wave, the (negative) scattering length is extremely sensitive to small differences in the strength of the force. The  $pp$  effective range parameters (scattering length,  $a$ , and effective range,  $r$ ) are obtained with very high precision from low-energy  $pp$  cross section data. However, since we are interested here in the strong force, electromagnetic effects have to be removed, which introduces model dependence. Using several realistic  $NN$  potential models, the pure strong-interaction  $pp$  effective range parameters are determined to be [2]

$$a_{pp}^N = -17.3 \pm 0.4 \text{ fm}, \quad (1)$$

$$r_{pp}^N = 2.85 \pm 0.04 \text{ fm}, \quad (2)$$

where the errors state the uncertainty due to model-dependence.

Since  $nn$  scattering experiments are not yet feasible, the  $nn$  effective range parameters are not measured directly; they are extracted from few-body reactions, mainly  $D(n, nn)p$  and  $D(\pi^-, \gamma)2n$ . Recent measurements of these reactions and their analysis have resulted in the following recommended values [1,2]

$$a_{nn}^N = -18.8 \pm 0.3 \text{ fm}, \quad (3)$$

$$r_{nn}^N = 2.75 \pm 0.11 \text{ fm}. \quad (4)$$

It is thus evident that in the  $^1S_0$  state, the  $nn$  strong interaction is slightly more attractive than the  $pp$  one. From the above semi-empirical values, we see that charge-symmetry is broken by the following amounts

$$\Delta a_{CSB} \equiv a_{pp}^N - a_{nn}^N = 1.5 \pm 0.5 \text{ fm}, \quad (5)$$

$$\Delta r_{CSB} \equiv r_{pp}^N - r_{nn}^N = 0.10 \pm 0.12 \text{ fm}. \quad (6)$$

Information about charge-symmetry-breaking (CSB) can also be inferred from binding energy differences of so-called mirror nuclei. The most studied case is the  $^3\text{He}$ – $^3\text{H}$  mirror pair. Experimentally it was found that  $^3\text{H}$  is more deeply bound than  $^3\text{He}$  by 764 keV. Model-independent calculations of the Coulomb energy difference and other subtle electromagnetic effects yield a binding energy difference of about  $683 \pm 29$  keV [5]. It has been shown that the remaining discrepancy can be explained by a charge symmetry breaking nuclear force that is consistent with the empirical asymmetry in the singlet scattering length [6].

According to our current understanding, CSB is due to a mass difference between the up and down quark and electromagnetic interactions. On the hadronic level, this has various consequences: mixing of mesons of different isospin but same spin and parity; mass differences between hadrons of the same isospin multiplet.

The difference between the masses of neutron and proton represents the most basic cause for CSB. Therefore, it is important to have a very thorough accounting of this effect. This is the subject of the present paper.

The  $n - p$  mass difference, which is well known to be 1.2933 MeV [9], affects the kinetic energy of the nucleons. Besides this, it has also an impact on all meson-exchange diagrams that contribute to the nuclear force.

In Sect. II, we will briefly outline the formalism of the Bonn model for the  $NN$  interaction that this study is based upon. In Sect. III, we will go—step by step—through the various meson-exchange contributions to the nuclear force and calculate for each step the CSB effect due to nucleon mass splitting. In particular, we will present the effect on the singlet effective range parameters and on phase shifts of  $NN$  scattering up to 300 MeV laboratory energy and up to orbital angular momentum  $L = 2$ . Section IV concludes the paper.

## II. SKETCH OF MODEL

We base our investigation on the comprehensive Bonn full model for the  $NN$  interaction. This model has been described in length in the literature [4,7,8]. Therefore, we will summarize here only those facts which are important for the issue under consideration.

The Bonn model uses an effective, field-theoretic approach, in which the interaction between two nucleons is created solely from the exchange of mesons; namely,  $\pi$ ,  $\rho(770)$ ,  $\omega(782)$ ,  $a_0/\delta(980)$ , and  $\sigma'(550)$ . Besides the nucleon, also the  $\Delta(1232)$  isobar is taken into account. In its original version [7], the Bonn model used averages for baryon and meson masses and, thus, was charge-independent; it was fitted to the neutron-proton data. In this paper, these subtleties will be treated accurately.

The interaction Lagrangians involving pions are

$$\mathcal{L}_{\pi NN} = \frac{f_{\pi NN}}{m_{\pi^\pm}} \bar{\psi} \gamma_\mu \gamma_5 \boldsymbol{\tau} \psi \cdot \partial^\mu \boldsymbol{\varphi}_\pi, \quad (7)$$

$$\mathcal{L}_{\pi N \Delta} = \frac{f_{\pi N \Delta}}{m_{\pi^\pm}} \bar{\psi} \boldsymbol{T} \psi_\mu \cdot \partial^\mu \boldsymbol{\varphi}_\pi + \text{H.c.}, \quad (8)$$

with  $\psi$  the nucleon,  $\psi_\mu$  the  $\Delta$  (Rarita-Schwinger spinor), and  $\boldsymbol{\varphi}_\pi$  the pion fields.  $\boldsymbol{\tau}$  are the usual Pauli matrices describing isospin 1/2 and  $\boldsymbol{T}$  is the isospin transition operator. H.c. denotes the Hermitean conjugate.

The above Lagrangians are divided by  $m_{\pi^\pm}$  to make the coupling constants  $f$  dimensionless. Following established conventions [10], we always use  $m_{\pi^\pm}$  as scaling mass. It may be tempting to use  $m_{\pi^0}$  for  $\pi^0$  coupling. Notice, however, that the scaling mass could be anything.

Therefore, it is reasonable to keep the scaling mass constant within SU(3) multiplets [10]. This avoids the creation of unmotivated charge-dependence.

It is important to stress that—as evidenced by the above  $\pi NN$  Lagrangian—we use the pseudovector (pv) or gradient coupling for the pion. Alternatively, one can also use the pseudoscalar (ps) coupling,

$$\mathcal{L}_{\pi NN}^{(ps)} = g_{\pi NN} \bar{\psi} i \gamma_5 \boldsymbol{\tau} \psi \cdot \boldsymbol{\varphi}_\pi. \quad (9)$$

For an on-shell process, the two couplings yield the same if the coupling constants are related by,

$$g_{\pi NN} = \left( \frac{M_1 + M_2}{m_{\pi^\pm}} \right) f_{\pi NN}, \quad (10)$$

with  $M_1$  and  $M_2$  the masses of the two nucleons involved. This relationship is charge-dependent due to the two nucleon masses. As a consequence, CSB effects will come out (noticeably!) different depending on if the ps or the pv coupling is used. Non-linear realizations of chiral symmetry, which are currently fashionable, prefer the pv coupling over the ps coupling. Following this trend, we use the pv coupling.

The couplings of  $\rho$ -mesons to nucleons and  $\Delta$ -isobars are described by the Lagrangians

$$\begin{aligned} \mathcal{L}_{\rho NN} &= g_{\rho NN} \bar{\psi} \boldsymbol{\gamma}_\mu \boldsymbol{\tau} \psi \cdot \boldsymbol{\varphi}_\rho^\mu \\ &+ \frac{f_{\rho NN}}{4M_p} \bar{\psi} \boldsymbol{\sigma}_{\mu\nu} \boldsymbol{\tau} \psi \cdot (\partial^\mu \boldsymbol{\varphi}_\rho^\nu - \partial^\nu \boldsymbol{\varphi}_\rho^\mu), \end{aligned} \quad (11)$$

$$\mathcal{L}_{\rho N\Delta} = i \frac{f_{\rho N\Delta}}{m_{\rho^\pm}} \bar{\psi} \boldsymbol{\gamma}_5 \boldsymbol{\gamma}_\mu \mathbf{T} \psi_\nu \cdot (\partial^\mu \boldsymbol{\varphi}_\rho^\nu - \partial^\nu \boldsymbol{\varphi}_\rho^\mu) + \text{H.c.} \quad (12)$$

We have to draw attention to the fact that—no matter to which nucleon the  $\rho$  couples—in the second part of the  $\rho NN$  Lagrangian, we always use the proton mass  $M_p$  as scaling mass. With this, we follow established conventions, as discussed above in conjunction with the pion Lagrangians. We note that disregarding this point would generate noticeable, but unmotivated CSB.

Finally, the Lagrangians for  $\omega$  and  $\sigma'$  are:

$$\mathcal{L}_{\omega NN} = g_{\omega NN} \bar{\psi} \boldsymbol{\gamma}_\mu \psi \varphi_\omega^\mu, \quad (13)$$

$$\mathcal{L}_{\sigma' NN} = g_{\sigma' NN} \bar{\psi} \psi \varphi_{\sigma'}. \quad (14)$$

Starting from these Lagrangians, irreducible diagrams up to fourth order are evaluated using old-fashioned/time-ordered perturbation theory. Some important diagrams (but not all) are shown in Figs. 1–4. The sum of all irreducible diagrams included in the model is, by definition, the quasi-potential  $V$ . Mathematically, this quasi-potential is the kernel of the scattering equation. For an uncoupled partial wave with angular momentum  $J$ , this equation reads:

$$R_J(q', q) = V_J(q', q) + \mathcal{P} \int_0^\infty \frac{dk k^2}{2E_q - 2E_k} V_J(q', k) R_J(k, q) \quad (15)$$

with  $q$ ,  $k$ , and  $q'$  the magnitude of the relative momenta of the two interacting nucleons in the initial, intermediate, and final state, respectively;  $E_q = \sqrt{M^2 + q^2}$  and  $E_k = \sqrt{M^2 + k^2}$  with  $M$  the correct mass of the nucleon involved in the scattering process under consideration. The principal value is denoted by  $\mathcal{P}$  and  $R$  is commonly called the K-matrix. By solving this equation, the kernel/quasi-potential is iterated infinitely many times. This is equivalent to solving the Schrodinger equation.

From the on-shell  $R$ -matrix, phase shifts for uncoupled partial waves are obtained through:

$$\tan \delta_J(T_{lab}) = -\frac{\pi}{2} q E_q R_J(q, q) \quad (16)$$

where  $q$  denotes the on-shell momentum in the center-of-mass system of the two nucleons which is related to the laboratory kinetic energy by  $T_{lab} = 2q^2/M$ .

Further details concerning the formalism can be found in appendices A to C of Ref. [7].

### III. CSB DUE TO NUCLEON MASS DIFFERENCE

It is the purpose of the present investigation to take the nucleon mass splitting accurately into account, which leads to CSB. Therefore, we use exact values for the proton mass  $M_p$  and neutron mass  $M_n$  [9]:

$$M_p = 938.2723 \text{ MeV}, \quad (17)$$

$$M_n = 939.5656 \text{ MeV}. \quad (18)$$

We start with  $pp$  scattering for which the one-boson-exchange contribution is depicted in Fig. 1b and  $2\pi$ -exchange contributions are shown in Fig. 2b, 3b, and 4b. Note that in all of these diagrams, the proton carries the exact proton mass  $M_p$  and the neutron, which occurs in some intermediate states, carries the exact neutron mass  $M_n$ . For the  $\Delta$ -isobars, that are excited in some intermediate states in Figs. 3 and 4, the average mass  $M_\Delta = 1232$  MeV is used.

For the  $pp$  case, our model yields  $-17.20$  fm for the singlet scattering length and  $2.88$  fm for the corresponding effective range, consistent with Eqs. (1) and (2).

Switching now—step by step—from  $pp$  to  $nn$  scattering will change the effective range parameters and the phase shifts, in violation of charge-symmetry.

The differences that occur for the effective range parameters are given in Table I and II. Note that the relationship between the CSB potential and the corresponding change of the scattering length,  $\Delta a_{CSB}$ , is highly non-linear. As discussed in Refs. [11,12], when the scattering length changes from  $a_1$  to  $a_2$  due to a CSB potential  $\Delta V = V_1 - V_2$ , the relationship is

$$\frac{1}{a_2} - \frac{1}{a_1} = M_N \int_0^\infty \Delta V u_1 u_2 dr \quad (19)$$

or

$$a_1 - a_2 = a_1 a_2 M_N \int_0^\infty \Delta V u_1 u_2 dr, \quad (20)$$

with  $u_1$  and  $u_2$  the zero-energy  $^1S_0$  wave functions normalized such that  $u(r \rightarrow \infty) \rightarrow (1 - r/a)$ . Thus, the perturbation expansion concerns the inverse scattering length. As clearly evident from Eq. (20), the change of the scattering length depends on the ‘‘starting value’’  $a_1$  to which the effect is added. In our calculations, CSB effects are generated step by step, which implies that the starting value  $a_1$  is different for different CSB effects. This distorts the relative size of the scattering length differences. To make the relative comparison meaningful, we have rescaled our results for  $\Delta a_{CSB}$  according to a prescription given by Ericson and Miller [11], which goes as follows. Assume the ‘‘starting value’’ for the scattering length is  $a_1$  and a certain CSB effect brings it up to  $a_2$ . Then, the resulting scattering length difference ( $a_1 - a_2$ ) is rescaled by

$$\Delta a = (a_1 - a_2) \frac{a_{pp} a_{nn}}{a_1 a_2} \quad (21)$$

with  $a_{pp} = -17.3$  fm and  $a_{nn} = -18.8$  fm. This will make  $\Delta a$  independent of the choice for  $a_1$ . The numbers given in Table I and II for  $\Delta a_{CSB}$  are all rescaled according to this prescription.

To state the effects of CSB on the  $NN$  phase shifts, we introduce for each  $LSJ$  state the CSB phase shift difference  $\Delta \delta_{CSB}^{LSJ}(T_{lab})$ , defined by

$$\Delta \delta_{CSB}^{LSJ}(T_{lab}) \equiv \delta_{nn}^{LSJ}(T_{lab}) - \delta_{pp}^{LSJ}(T_{lab}) \quad (22)$$

where  $\delta_{nn}^{LSJ}$  denotes the  $nn$  and  $\delta_{pp}^{LSJ}$  the  $pp$  phase shifts (without electromagnetic effects), respectively.

The irreducible diagrams included in the quasi-potential/kernel can be subdivided into several groups. After discussing the effect from the kinetic energy, we will describe each group of diagrams and the implications for CSB.

**1. Kinetic energy (kin. en.).** The kinetic energy is smaller for the neutron because of its larger mass. This reduces the magnitude of the energy-denominator in Eq. (15) for  $nn$  scattering as compared to  $pp$ , thus, enhancing the (attractive) integral term for  $nn$ . In addition, the factor  $E_q$  in Eq. (16) is larger for the larger nucleon mass, which results in an overall enhancement of the magnitude of the  $nn$  phase shifts. The combined effect yields larger  $nn$  phase shifts as compared to  $pp$  if the nuclear potential is attractive, and vice versa if the nuclear potential is repulsive. This can be understood more easily in the frame work of the radial Schroedinger equation in which the effective potential is  $MV$ . Thus, no matter if the nuclear potential  $V$  is attractive or repulsive, its effect on the

phase shifts is always enhanced for the larger nucleon mass  $M$ . This explains why in  $^3P_1$  the CSB phase shift splitting, Eq. (22), comes out negative (repulsive potential, negative phase shift), while it is positive in all other partial waves listed in Table III (column ‘kin.en.’) where the potentials are attractive (positive phase shifts). The magnitude of the singlet scattering length increases by 0.25 fm (cf. Table I, column ‘kin.en.’) for  $nn$  scattering as compared to  $pp$ . This is, of course, well known, and the effect on the scattering length is usually quoted to be 0.30 fm [13]. Our value is slightly smaller which can be attributed to the use of relativistic kinetic energies in our model.

2. **One-boson-exchange (OBE, Fig. 1)** contributions mediated by  $\pi^0(135)$ ,  $\rho^0(770)$ ,  $\omega(782)$ ,  $a_0/\delta(980)$ , and  $\sigma'(550)$ . In the Bonn model [7], the  $\sigma'$  describes only the correlated  $2\pi$  exchange in  $\pi\pi - S$ -wave (and not the uncorrelated  $2\pi$  exchange since the latter is calculated explicitly, cf. Figs. 2–4). Charge-symmetry is broken by the fact that for  $pp$  scattering the proton mass is used in the Dirac spinors representing the four external legs (Fig. 1b), while for  $nn$  scattering the neutron mass is applied (Fig. 1a). The CSB effect from the OBE diagrams is extremely small (cf. Table I and III, column ‘OBE’).
3.  **$2\pi$ -exchange with  $NN$  intermediate states ( $2\pi NN$ ), Fig 2.** Notice first that only non-iterative diagrams are to be considered, since the iterative ones are generated by the scattering equation (15) from the OBE diagrams. In our calculations, we include always all time-orderings (except those with anti-baryons in intermediate states); to save space, we display, however, only a few characteristic graphs in Fig. 2 (this is also true for all diagrams shown or discussed below). Part (a) of Fig. 2 applies to  $nn$  scattering, while part (b) refers to  $pp$  scattering. Notice that when charged-pion exchange is involved, the intermediate-state nucleon differs from that of the external legs. This is an important subtlety that we account for accurately in our calculations; neglecting this effect causes a systematic error in the order of 100%. Numerical results for this class of diagrams are given in Table II and IV, column ‘ $2\pi NN$ ’.
4.  **$2\pi$ -exchange with  $N\Delta$  intermediate states ( $2\pi N\Delta$ ), Fig. 3.** This class of diagrams causes by far the largest CSB effect on the scattering length (Table II) as well as on the phase shifts (Table IV). Again, it is important in all of these diagrams to take the intermediate-state nucleon mass correctly into account.
5.  **$2\pi$ -exchange with  $\Delta\Delta$  intermediate states ( $2\pi\Delta\Delta$ ), Fig. 4.** The effects are smaller than for

$2\pi N\Delta$  because there are no nucleon intermediate states. Thus, the nucleon mass splitting affects only the outer legs which typically results in a small effect.

6.  **$\pi\rho$ -exchange with  $NN$  intermediate states** ( $\pi\rho NN$ ). Graphically, the  $\pi\rho NN$  diagrams can be obtained by replacing in each diagram of Fig. 2, one pion by a  $\rho$ -meson of the same charge state (because of this simple analogy, we do not show the  $\pi\rho$  diagrams explicitly here). In our calculations, the CSB effects of the  $\pi\rho$  diagrams with  $NN$  intermediate states are taken into account accurately. The effect is typically opposite to the one from  $2\pi NN$  exchange.
7.  **$\pi\rho$ -exchange with  $N\Delta$  intermediate states** ( $\pi\rho N\Delta$ ). Concerning the  $\pi\rho$  diagrams with  $\Delta$  intermediate states a comment is in place. In the Bonn model [7], the crossed  $\pi\rho$  diagrams with  $\Delta$  intermediate states are included in terms of an approximation. It is assumed that they differ from the corresponding box diagrams (i. e., the diagrams on the left-hand side of Figs. 3 and the ones in the first row of Fig. 4a and 4b, but with one  $\pi$  replaced by one  $\rho$ ) only by the isospin factor. Thus, the  $\pi\rho$  box diagrams with  $\Delta$  intermediate states are multiplied by an isospin factor that is equal to the sum of the isospin factors for box and crossed box. The  $\pi\rho N\Delta$  effect is in general substantial and typically of the opposite sign as compared to  $2\pi N\Delta$ .
8.  **$\pi\rho$ -exchange with  $\Delta\Delta$  intermediate states** ( $\pi\rho\Delta\Delta$ ). The effects are very small.
9. **Further  $3\pi$  and  $4\pi$  contributions** ( $\pi\sigma + \pi\omega$ ). The Bonn potential also includes some  $3\pi$ -exchanges that can be approximated in terms of  $\pi\sigma$  diagrams and  $4\pi$ -exchanges of  $\pi\omega$  type. The sum of these contributions is small. These diagrams have  $NN$  intermediate states (similar to Fig. 2, but with one of the two exchanged pions replaced by an isospin-zero boson) and, thus, are of intermediate range. Except for  $^1S_0$ , their effect is negligible.

This finishes our detailed presentation of the relevant diagrams and their CSB effects which are plotted in Figs. 5 and 6. The total CSB splitting of the singlet scattering length amounts to 1.58 fm (cf. last column of Table I) which agrees well with the empirical value  $1.5 \pm 0.5$  fm, Eq. (5). The sum of all CSB effects on phase shifts is given in the last column of Table III and plotted by the solid curve in Fig. 5. The largest total effect listed in Table III is 1.8 deg in  $^1S_0$  at 1 MeV. In the  $S$ -wave, the effect decreases with energy and is 0.15 deg at 300 MeV. In  $P$  and  $D$  waves the CSB effect on phase shifts increases with energy and is typically in the order of 0.1 deg at 300 MeV. We do not list our results for partial waves with  $L \geq 3$ , since the CSB effect becomes negligibly small for high  $L$ : less than 0.02 deg at

300 MeV and 0.01 deg or less at 200 MeV for  $F$  and  $G$  waves and even smaller for higher partial waves.

Since the pion is involved in almost all diagrams considered in this study, the CSB effect depends on the  $\pi NN$  coupling constant. In the present calculations, we follow the Bonn model [7]: we assume charge-independence of the coupling constant and use  $f_{\pi NN}^2/4\pi = 0.0795$  which, via Eq. (10), translates into  $g_{\pi NN}^2/4\pi = 14.4$ . In recent years, there has been some controversy about the precise value of the  $\pi NN$  coupling constant. Unfortunately, the problem is far from being settled. Based upon  $NN$  phase shift analysis, the Nijmegen group [14] advocates the ‘small’ charge-independent value  $g_{\pi}^2/4\pi = 13.5(1)$ , while a very recent determination by the Uppsala group [15] based upon high precision  $np$  charge-exchange data at 162 MeV seems to confirm in the large ‘text book’ value  $g_{\pi^\pm}^2/4\pi = 14.5(3)$ . Other recent determinations are in-between the two extremes: The VPI group [16] quotes  $g_{\pi}^2/4\pi = 13.77(15)$  from  $\pi N$  and  $NN$  analysis with no evidence for charge-dependence. Bugg and Machleidt [17] obtain  $g_{\pi^\pm}^2/4\pi = 13.69(39)$  and  $g_{\pi^0}^2/4\pi = 13.94(24)$  from the analysis of  $NN$  elastic data between 210 and 800 MeV. Because of this large uncertainty in the  $\pi NN$  coupling constant, it is of interest to know how the CSB effects depends on this constant. Naturally, the  $2\pi$  contributions are proportional to  $g_{\pi}^4$  [18] and the  $\pi\rho$  ones to  $g_{\pi}^2$ . Since the two contributions carry (in general) opposite signs and vary in their relative magnitude from partial wave to partial wave, there is no simple rule for how the total CSB effect depends on  $g_{\pi}$ . The value  $g_{\pi}^2/4\pi = 13.6$  is currently fashionable among the new generation of high-precision  $NN$  potentials [19–21]. For that reason, we have repeated our CSB calculations using  $g_{\pi}^2/4\pi = 13.6$  and find that the total  $\Delta a_{CSB}$  is reduced by about 15% as compared to the calculation using  $g_{\pi}^2/4\pi = 14.4$  (Table I). The phase shift differences are reduced by roughly the same percentage in most partial waves. The exact numbers for  $g_{\pi}^2/4\pi = 13.6$  will be published elsewhere.

#### IV. SUMMARY AND CONCLUSIONS

Based upon the Bonn meson-exchange model for the  $NN$  interaction, we have calculated the CSB effects due to nucleon mass splitting on the phase shifts of  $NN$  scattering and the singlet effective range parameters. We give results for partial waves up to  $L = 2$  and laboratory energies below 300 MeV.

A remarkable finding is that the experimental CSB difference in the singlet scattering length can be explained from nucleon mass splitting alone.

Concerning phase shift differences, we find the largest in the  $^1S_0$  state where they are most noticeable at low energy; e. g., at 1 MeV, the difference is 1.8 deg, indicating that the  $nn$  nuclear force is more attractive than the  $pp$  one. The  $^1S_0$  phase shift difference decreases with

increasing energy and is about 0.15 deg at 300 MeV.

The CSB effect on the phase shifts of higher partial waves is small; in  $P$  and  $D$  waves, typically in the order of 0.1 deg at 300 MeV and less at lower energies. This is substantially smaller than what is required phenomenologically to solve the so-called  $A_y$  puzzle in elastic nucleon-deuteron scattering at low energies [22].

The major part of the CSB effect comes from diagrams of  $2\pi$  exchange where those with  $N\Delta$  intermediate states make the largest contribution. We also study the CSB effect from irreducible diagrams that exchange a  $\pi$  and  $\rho$  meson. To our knowledge, this class of diagrams has never before been considered in any calculation of the CSB nuclear force. We find that the  $\pi\rho$  diagrams give rise to non-negligible CSB contributions that are typically opposite to the  $2\pi$  effects. In most partial waves, the  $\pi\rho$  effect reduces the CSB from  $2\pi$  exchange in the order of 50%.

Coon and Niskanen [23] have investigated the CSB effect on the singlet scattering length from the diagrams of Figs. 2 and 3, using a nonrelativistic model. Their total result,  $\Delta a_{CSB} = 1.56$  fm (applying the dTRS  $NN$  potential [24] and a cutoff mass of 1 GeV at the pion vertices), agrees well with our total. However, there are large differences in the details: from  $2\pi NN$  and  $2\pi N\Delta$ , Coon and Niskanen obtain 1.28 fm and 0.24 fm, respectively; while we get 0.37 fm and 1.85 fm, respectively. Thus, the ratio of the two contributions is very different. From Ref. [7] it is known, that the  $2\pi N\Delta$  contribution to the nuclear force is about four times the one from  $2\pi NN$ . It is reasonable to expect that the CSB effect scales roughly with the size of the contribution that generates it. This is true for our result, which is why we have confidence in our findings. In the Bonn model, a cutoff mass of 1.2 GeV is used at the pion vertices, while Coon and Niskanen use 1 GeV. This may explain why our overall contribution from  $2\pi$  exchange is larger. On the other hand, our model also includes the important  $\pi\rho$  diagrams (that are omitted in Ref. [23]), which reduce the overall CSB effect.

From the diagrams displayed in Figs. 3 and 4 it is evident that additional CSB could be created from  $\Delta$ -mass splitting. Unfortunately, the charge-splitting of the  $\Delta(1232)$ -baryon mass is not well known [9]. Since our present investigation is restricted to reliably known baryon-mass splitting, we do not consider any  $\Delta$ -mass splitting and use the average value for the  $\Delta$ -mass (1232 MeV) throughout. It is, however, worthwhile to mention that our model includes everything needed for a systematic investigation of CSB effects caused by an assumed  $\Delta$ -mass splitting. This may be an interesting topic for a future study.

Traditionally, it was believed that  $\rho^0 - \omega$  mixing explains essentially all CSB in the nuclear force. However, recently some doubt has been cast on this paradigm. Some researchers [25–27] found that  $\rho^0 - \omega$  exchange may have a substantial  $q^2$  dependence such as to cause this contribution to nearly vanish in  $NN$ . Our finding that the empirically known CSB in the nuclear force can be

explained solely from nucleon mass splitting (leaving essentially no room for additional CSB contributions from  $\rho^0 - \omega$  mixing or other sources) fits well into this new scenario. However, since the issue of the  $q^2$  dependence of  $\rho^0 - \omega$  exchange is by no means settled (see Ref. [3] for discussion and more references), it is premature to draw any definite conclusions.

This work was supported in part by the U.S. National Science Foundation under Grant No. PHY-9603097 and by the Idaho State Board of Education.

- 
- [1] I. Slaus, Y. Akaishi and H. Tamaka, Phys. Rep. **173** 257 (1989).
- [2] G. A. Miller, B. M. K. Nefkens and I. Slaus, Phys. Rep. **194**, 1 (1990).
- [3] G. A. Miller and W. H. T. van Oers, In *Symmetries and Fundamental Interactions in Nuclei*, W. C. Haxton and E. M. Henley, eds. (World Scientific, Singapore, 1995) p. 127.
- [4] R. Machleidt, Adv. Nucl. Phys. **19**, 189 (1989).
- [5] R. A. Brandenburg, S. A. Coon and P. U. Sauer, Nucl. Phys. **A294**, 305 (1978).
- [6] R. A. Brandenburg, G. S. Chulick, Y. E. Kim, D. J. Klepacki, R. Machleidt, A. Picklesimer and R. M. Thaler, Phys. Rev. **C37**, 781 (1988).
- [7] R. Machleidt, K. Holinde, and Ch. Elster, Phys. Reports **149**, 1 (1987).
- [8] R. Machleidt and G. Q. Li, Phys. Reports **242**, 5 (1994).
- [9] Particle Data Group, Review of Particle Properties, Phys. Rev. D **45** (1992).
- [10] O. Dumbrajs *et al.*, Nucl. Phys. **B216**, 277 (1983).
- [11] T. E. O. Ericson and G. A. Miller, Phys. Lett. **132B**, 32 (1983).
- [12] C. Y. Cheung and R. Machleidt, Phys. Rev. C **34** 1181 (1986).
- [13] E. M. Henley, in *Isospin in Nuclear Physics*, D. H. Wilkinson, ed. (North-Holland, Amsterdam, 1969), p. 16.
- [14] V. Stoks, R. Timmermans, and J. J. de Swart, Phys. Rev. C **47**, 512 (1993).
- [15] T. E. O. Ericson *et al.*, Phys. Rev. Lett. **75**, 1046 (1995); J. Rahm *et al.*, Phys. Rev. C **57**, 1077 (1998).
- [16] R. A. Arndt, R. L. Workman, and M. M. Pavan, Phys. Rev. C **49**, 2729 (1994); R. A. Arndt, I. I. Strakovsky, and R. L. Workman, *ibid.*, **52**, 2246 (1995).
- [17] D. V. Bugg and R. Machleidt, Phys. Rev. C **52**, 1203 (1995).
- [18] Note that in the Bonn model [7]  $f_{\pi N\Delta}$  depends on  $f_{\pi NN}$  via the  $SU(3)$  based relationship
- $$f_{\pi N\Delta}^2 = \frac{72}{25} f_{\pi NN}^2 .$$
- [19] R. Machleidt, F. Sammarruca, and Y. Song, Phys. Rev. **53**, 1483 (1996).
- [20] R.B. Wiringa, V.G.J. Stoks, and R. Schiavilla, Phys. Rev. C **51**, 38 (1995).
- [21] V.G.J. Stoks, R.A.M. Klomp, C.P.F. Terheggen, and J.J. de Swart, Phys. Rev. C **49**, 2950 (1994).
- [22] H. Witala and W. Glöckle, Nucl. Phys. **A528**, 48 (1991); W. Glöckle, H. Witala, D. Hüber, H. Kamada, and J. Golak, Phys. Reports **274**, 107 (1996); D. Hueber and J. L. Friar, *The  $A_y$  Puzzle and the Nuclear Force*, nucl-th/9803038.
- [23] S. A. Coon and J. A. Niskanen, Phys. Rev. C **53**, 1154 (1996).
- [24] R. de Tourreil, B. Rouben, and D. W. L. Sprung, Nucl. Phys. **A242**, 445 (1975).
- [25] T. Goldman, J. A. Henderson, and A. W. Thomas, Few-Body Systems **12**, 193 (1992).
- [26] J. Piekarewicz and A. G. Williams, Phys. Rev. C **47**, 2462 (1993).
- [27] G. Krein, A. W. Thomas, and A. G. Williams, Phys. Lett. **B317**, 293 (1993).

TABLE I. CSB differences of the  $^1S_0$  effective range parameters as explained in the text.  $2\pi$  denotes the sum of all  $2\pi$ -contributions and  $\pi\rho$  the sum of all  $\pi\rho$ -contributions. TBE (non-iterative two-boson-exchange) is the sum of  $2\pi$ ,  $\pi\rho$ , and  $(\pi\sigma + \pi\omega)$ .

	kin. en.	OBE	$2\pi$	$\pi\rho$	$\pi\sigma + \pi\omega$	TBE	Total
$\Delta a_{CSB}$ (fm)	0.246	0.013	2.888	-1.537	-0.034	1.316	1.575
$\Delta r_{CSB}$ (fm)	0.004	0.001	0.055	-0.031	-0.001	0.023	0.027

TABLE II. CSB differences of the  $^1S_0$  effective range parameters from  $2\pi$  and  $\pi\rho$  diagrams as explained in the text.

	$2\pi NN$	$2\pi N\Delta$	$2\pi\Delta\Delta$	$\pi\rho NN$	$\pi\rho N\Delta$	$\pi\rho\Delta\Delta$	Sum
$\Delta a_{CSB}$ (fm)	0.374	1.852	0.662	-0.484	-1.184	0.130	1.350
$\Delta r_{CSB}$ (fm)	0.005	0.036	0.014	-0.010	-0.025	0.003	0.024

TABLE III. CSB phase shift differences (in degrees) as defined in Eq. (22). Notation as in Table I.

$T_{lab}$ (MeV)	kin. en.	OBE	$2\pi$	$\pi\rho$	$\pi\sigma + \pi\omega$	TBE	Total
$^1S_0$							
1	0.287	0.015	3.417	-1.856	-0.041	1.520	1.822
5	0.162	0.010	1.850	-1.007	-0.022	0.810	0.982
10	0.104	0.006	1.409	-0.773	-0.018	0.618	0.727
25	0.066	0.004	0.995	-0.585	-0.014	0.396	0.466
50	0.053	0.003	0.778	-0.460	-0.011	0.291	0.347
100	0.036	0.004	0.585	-0.378	-0.008	0.199	0.239
150	0.019	0.006	0.567	-0.387	-0.006	0.174	0.198
200	0.015	0.021	0.565	-0.407	-0.004	0.154	0.190
300	0.005	0.029	0.562	-0.446	-0.001	0.116	0.149
$^3P_0$							
5	0.004	0.003	0.001	0.000	0.000	0.001	0.009
10	0.010	0.006	0.001	0.001	0.000	0.002	0.019
25	0.020	0.014	0.003	0.003	0.001	0.007	0.042
50	0.025	0.018	0.006	0.006	0.002	0.014	0.057
100	0.025	0.014	0.008	0.010	0.003	0.021	0.060
150	0.016	0.017	0.007	0.012	0.004	0.023	0.057
200	0.008	0.022	0.006	0.014	0.005	0.024	0.054
300	0.004	0.023	0.002	0.016	0.005	0.022	0.050
$^3P_1$							
5	-0.002	-0.001	0.002	-0.001	0.000	0.001	-0.002
10	-0.004	-0.001	0.006	-0.002	0.000	0.004	-0.002
25	-0.011	0.001	0.017	-0.006	0.000	0.011	0.000
50	-0.017	0.002	0.044	-0.019	0.000	0.025	0.010
100	-0.025	0.008	0.092	-0.046	0.000	0.045	0.028
150	-0.033	0.016	0.139	-0.081	0.000	0.058	0.041
200	-0.041	0.023	0.185	-0.112	0.001	0.074	0.056
300	-0.059	0.033	0.278	-0.195	0.001	0.084	0.058
$^1D_2$							
25	0.001	0.001	0.002	0.000	0.000	0.002	0.004
50	0.004	0.001	0.008	-0.001	0.000	0.007	0.012
100	0.007	0.002	0.031	-0.007	0.000	0.024	0.033
150	0.011	0.003	0.061	-0.018	0.000	0.043	0.057
200	0.012	0.003	0.095	-0.034	0.000	0.061	0.076
300	0.014	0.003	0.178	-0.078	0.000	0.100	0.117
$^3P_2$							
5	0.001	0.000	0.002	0.000	0.000	0.002	0.003
10	0.002	0.001	0.006	-0.001	0.000	0.005	0.007
25	0.005	0.002	0.023	-0.006	0.000	0.018	0.025
50	0.014	0.002	0.054	-0.015	0.000	0.040	0.056
100	0.023	0.001	0.114	-0.036	0.001	0.079	0.102
150	0.026	0.001	0.154	-0.055	0.002	0.101	0.128
200	0.025	0.000	0.177	-0.068	0.003	0.112	0.137
300	0.023	0.000	0.237	-0.095	0.003	0.144	0.167

TABLE IV. CSB phase shift differences (in degrees) as defined in Eq. (22) from the various  $2\pi$  and  $\pi\rho$ -exchange contributions as defined in the text.

$T_{lab}$ (MeV)	$2\pi NN$	$2\pi N\Delta$	$2\pi\Delta\Delta$	$\pi\rho NN$	$\pi\rho N\Delta$	$\pi\rho\Delta\Delta$	Sum
$^1S_0$							
1	0.424	2.184	0.808	-0.592	-1.418	0.154	1.561
5	0.224	1.190	0.436	-0.317	-0.776	0.086	0.843
10	0.164	0.909	0.336	-0.242	-0.597	0.067	0.636
25	0.099	0.648	0.248	-0.182	-0.452	0.049	0.410
50	0.059	0.514	0.204	-0.138	-0.366	0.044	0.318
100	0.012	0.406	0.168	-0.105	-0.317	0.044	0.207
150	-0.005	0.392	0.180	-0.106	-0.331	0.049	0.180
200	-0.020	0.395	0.190	-0.108	-0.360	0.061	0.158
300	-0.065	0.405	0.223	-0.113	-0.413	0.080	0.117
$^3P_0$							
5	-0.001	0.001	0.000	0.000	0.000	0.000	0.001
10	-0.003	0.004	0.001	0.000	0.001	0.000	0.002
25	-0.012	0.013	0.002	0.000	0.003	-0.001	0.006
50	-0.022	0.024	0.004	0.001	0.006	-0.001	0.012
100	-0.036	0.038	0.006	0.001	0.011	-0.002	0.018
150	-0.044	0.044	0.007	0.000	0.014	-0.003	0.019
200	-0.051	0.049	0.008	0.000	0.017	-0.003	0.019
300	-0.064	0.057	0.009	-0.003	0.022	-0.004	0.017
$^3P_1$							
5	0.001	0.001	0.000	0.000	0.000	0.000	0.001
10	0.002	0.003	0.000	-0.001	-0.001	0.000	0.004
25	0.006	0.011	0.001	-0.002	-0.004	0.000	0.011
50	0.013	0.029	0.002	-0.006	-0.013	0.000	0.025
100	0.024	0.063	0.005	-0.014	-0.032	0.000	0.046
150	0.032	0.100	0.007	-0.024	-0.056	-0.001	0.059
200	0.038	0.139	0.009	-0.036	-0.074	-0.002	0.073
300	0.050	0.217	0.011	-0.051	-0.143	-0.001	0.083
$^1D_2$							
25	0.001	0.001	0.000	0.000	0.000	0.000	0.002
50	0.003	0.005	0.000	0.000	-0.001	0.000	0.007
100	0.010	0.019	0.002	-0.002	-0.005	0.000	0.024
150	0.016	0.041	0.003	-0.004	-0.013	0.000	0.043
200	0.021	0.071	0.004	-0.005	-0.029	0.000	0.061
300	0.027	0.142	0.009	-0.011	-0.065	-0.001	0.100
$^3P_2$							
5	0.000	0.001	0.000	0.000	0.000	0.000	0.002
10	0.001	0.004	0.001	0.000	-0.001	0.000	0.005
25	0.003	0.015	0.006	-0.002	-0.003	-0.001	0.018
50	0.005	0.035	0.014	-0.005	-0.007	-0.003	0.039
100	0.006	0.075	0.033	-0.013	-0.016	-0.007	0.078
150	0.005	0.102	0.047	-0.019	-0.025	-0.011	0.099
200	0.003	0.120	0.054	-0.022	-0.032	-0.014	0.109
300	-0.001	0.155	0.083	-0.031	-0.044	-0.021	0.142

FIG. 1. One-boson-exchange (OBE) contributions to (a)  $nn$  and (b)  $pp$  scattering.

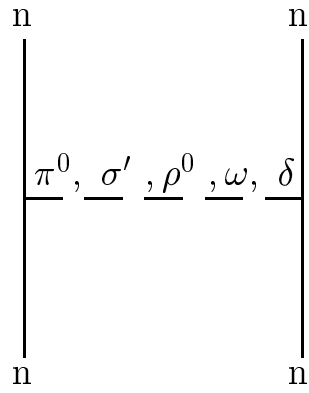
FIG. 2. Irreducible  $2\pi$ -exchange diagrams with  $NN$  intermediate states for (a)  $nn$  and (b)  $pp$  scattering.

FIG. 3.  $2\pi$ -exchange contributions with  $N\Delta$  intermediate states to (a)  $nn$  and (b)  $pp$  scattering.

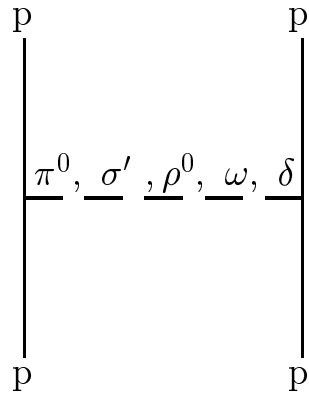
FIG. 4.  $2\pi$ -exchange contributions with  $\Delta\Delta$  intermediate states to (a)  $nn$  and (b)  $pp$  scattering.

FIG. 5. CSB phase shift differences  $\Delta\delta_{CSB}^{LSJ}$  (in degrees) as defined in Eq. (22) for laboratory kinetic energies  $T_{lab}$  below 300 MeV and partial waves with  $L \leq 2$ . The CSB effects due to the kinetic energy, OBE, the entire  $2\pi$  model, and  $\pi\rho$  exchanges are shown by the dotted, dash-triple-dot, dashed, and dash-dot curves, respectively. The solid curve is the sum of all CSB effects. (See text for further explanations.)

FIG. 6. Similar to Fig. 5, but here the individual contributions from the  $2\pi$  and  $\pi\rho$  exchange are shown. The CSB effects due to the  $2\pi NN$ ,  $2\pi N\Delta$ ,  $2\pi\Delta\Delta$ ,  $\pi\rho NN$ , and  $(\pi\rho N\Delta + \pi\rho\Delta\Delta)$  diagrams are shown by the dashed, solid, dotted, dash-dot, and dash-triple-dot curves, respectively. (See text for further explanations.)

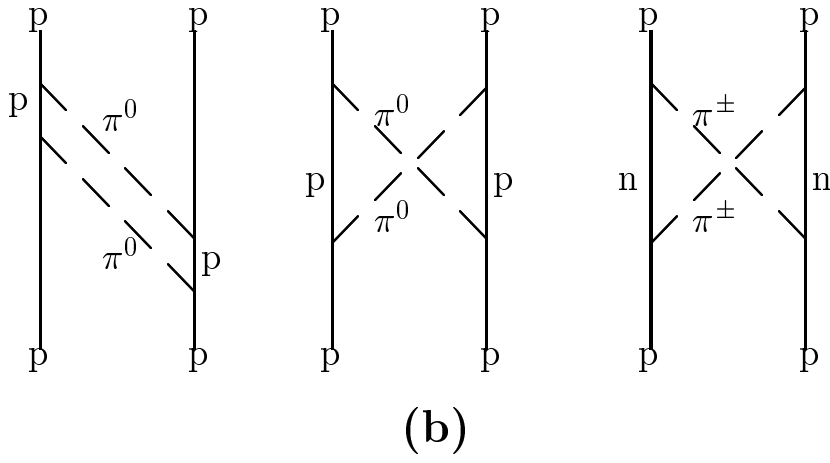
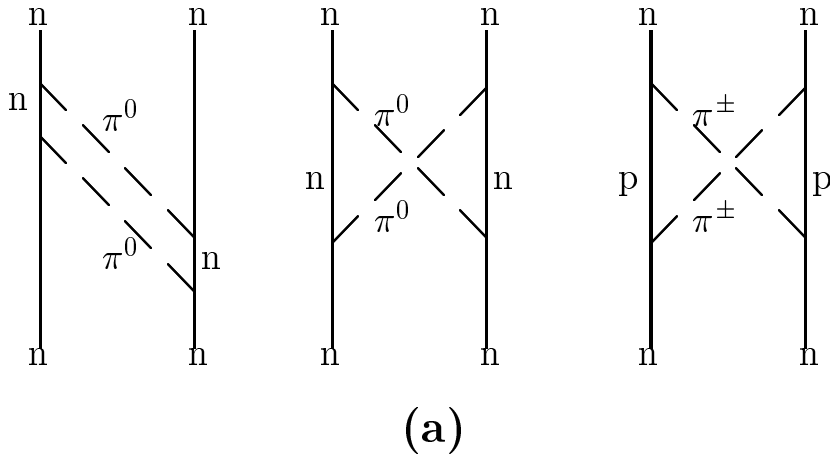


**(a)**

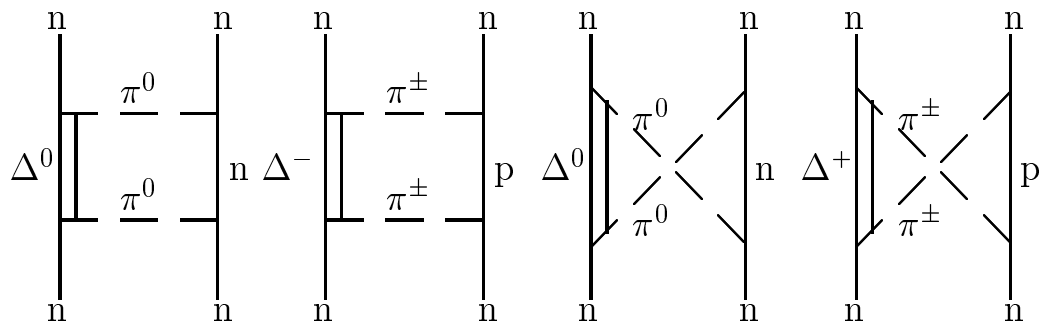


**(b)**

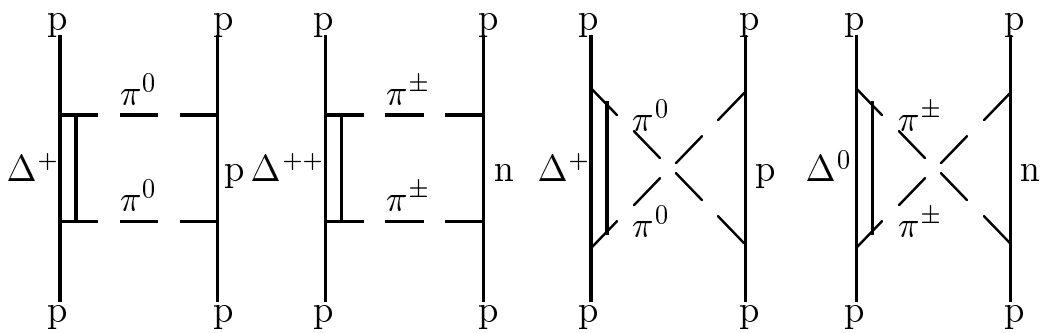
Li/Machleidt (CSB) Fig. 1



Li/Machleidt (CSB) Fig. 2

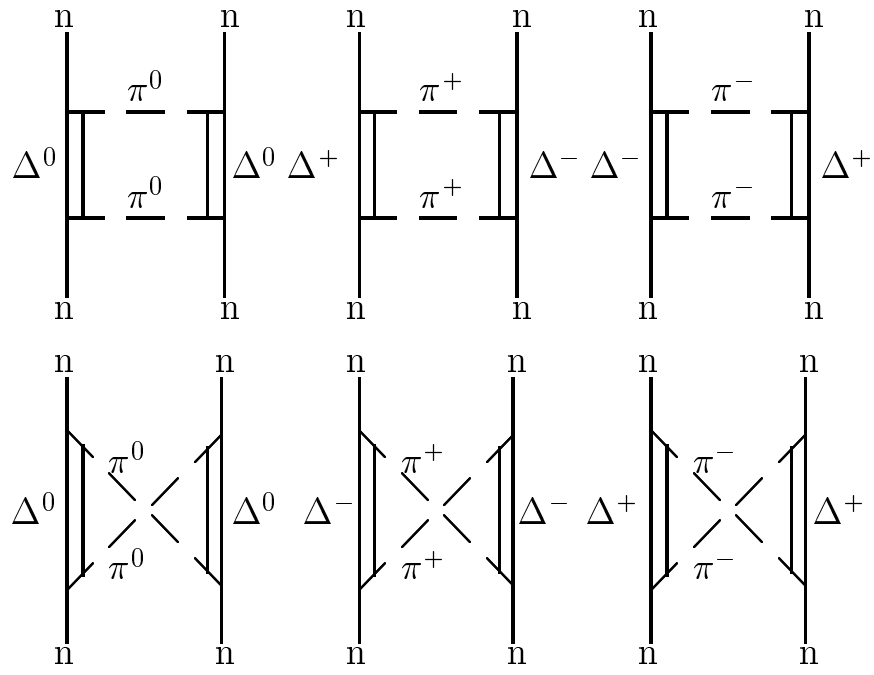


(a)

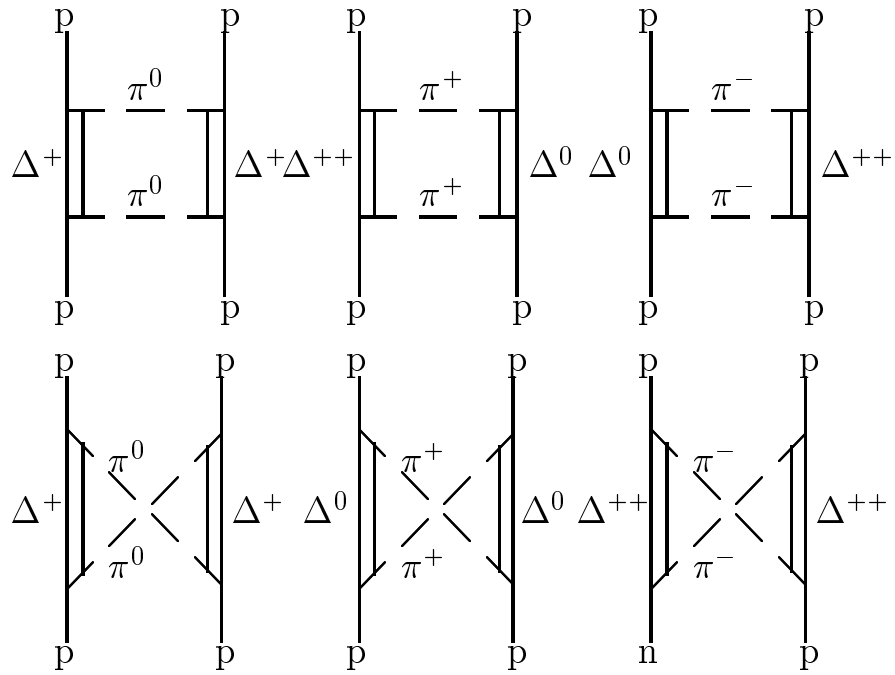


(b)

Li/Machleidt (CSB) Fig. 3

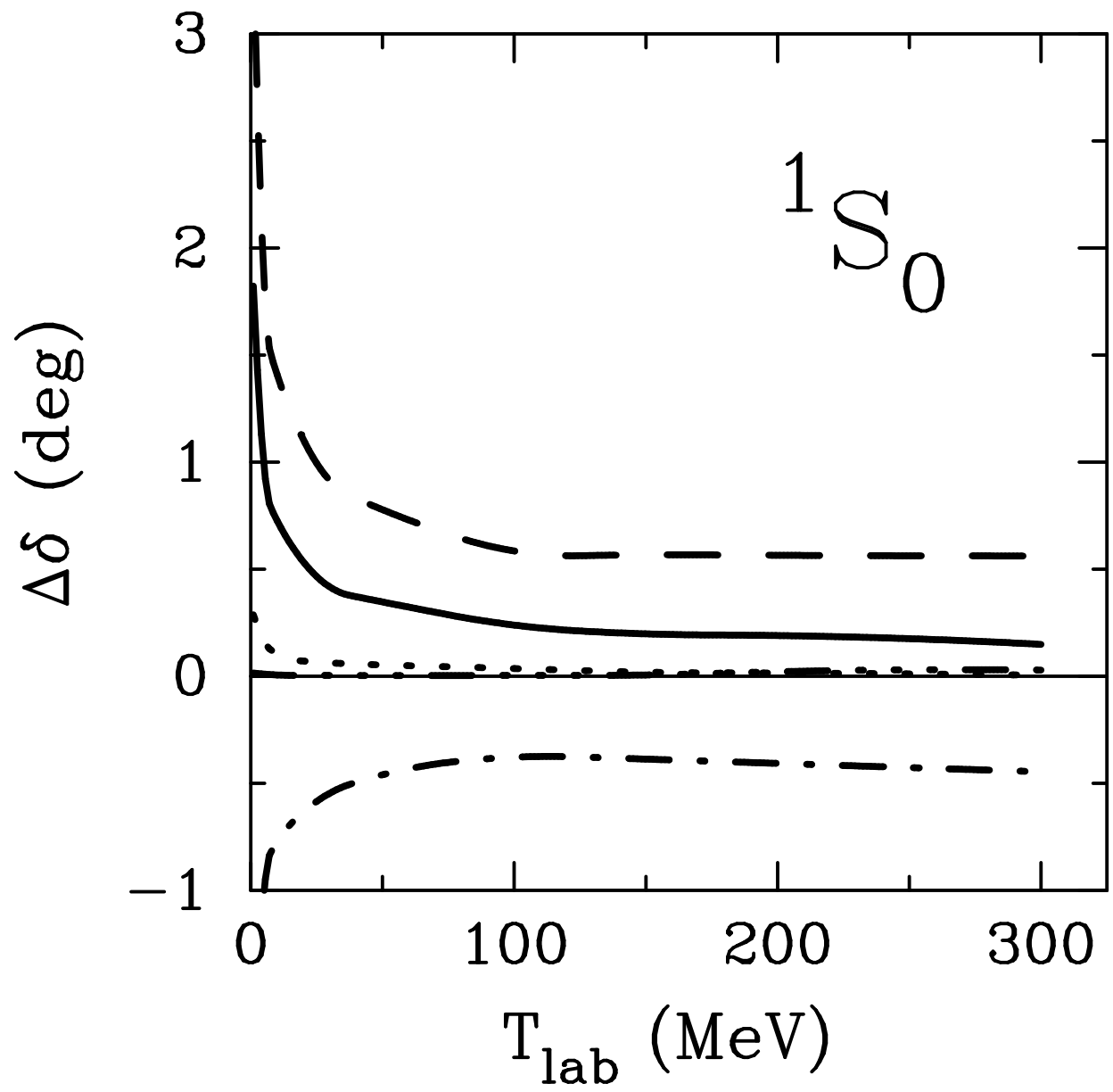


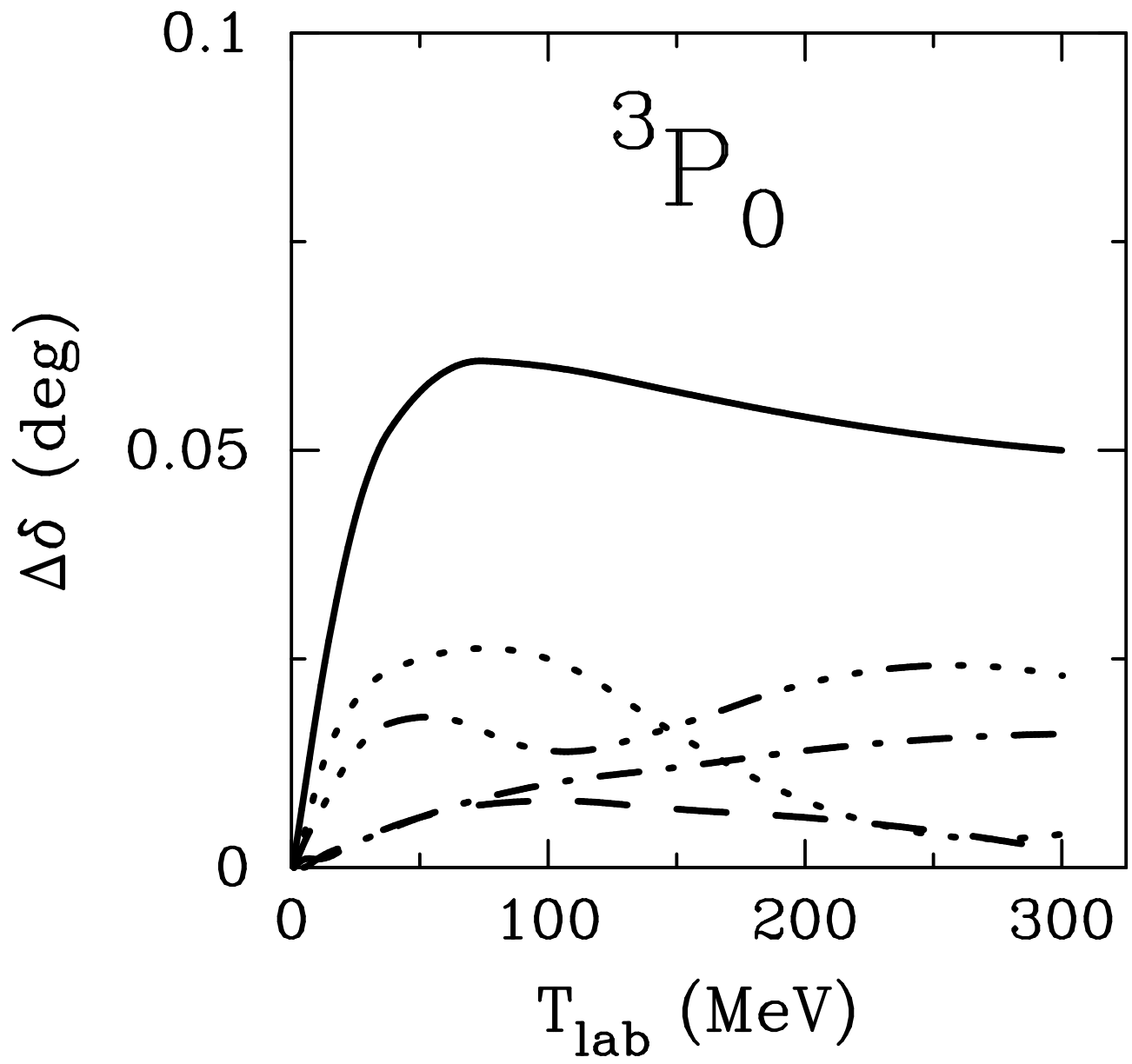
(a)

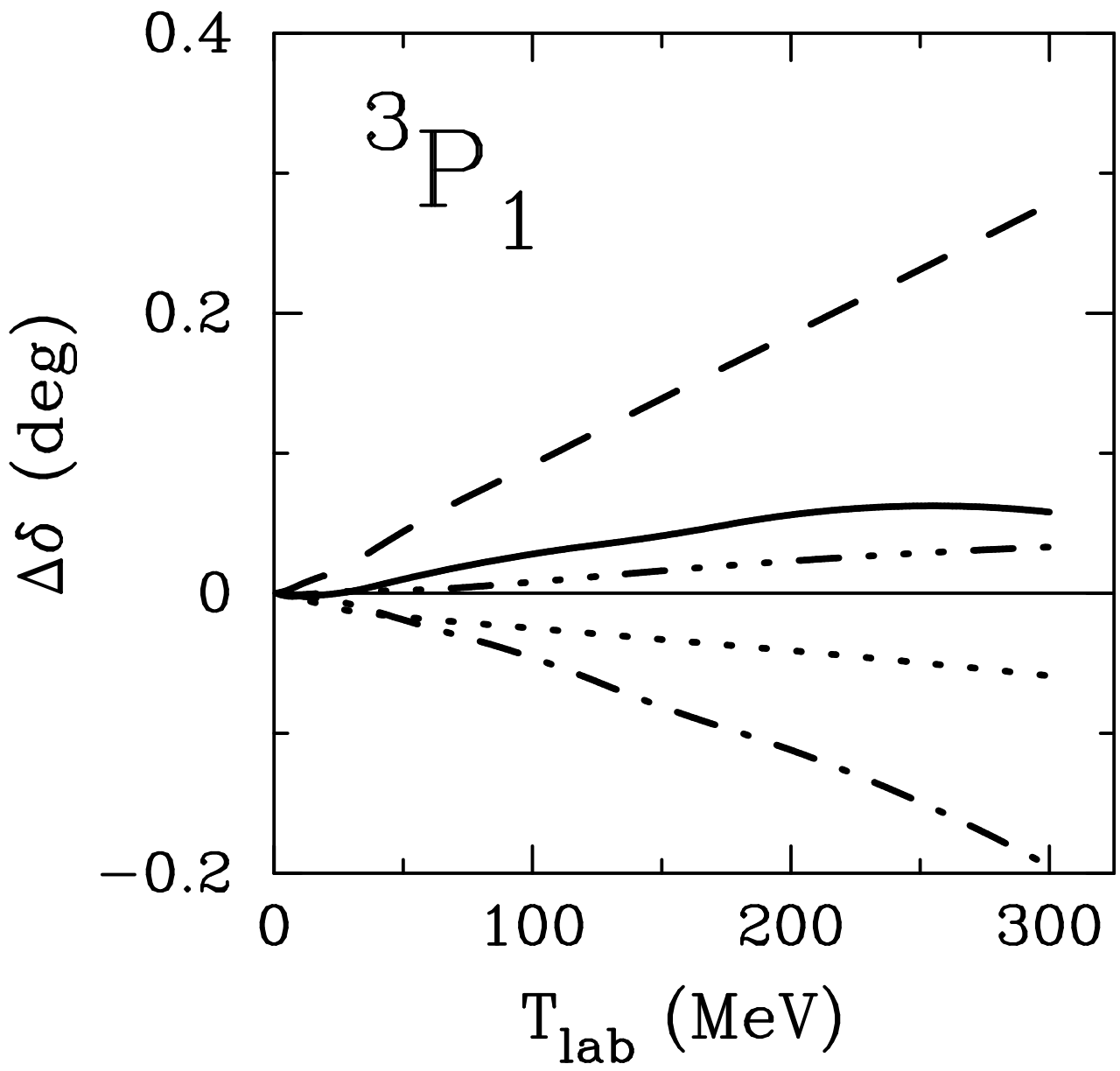


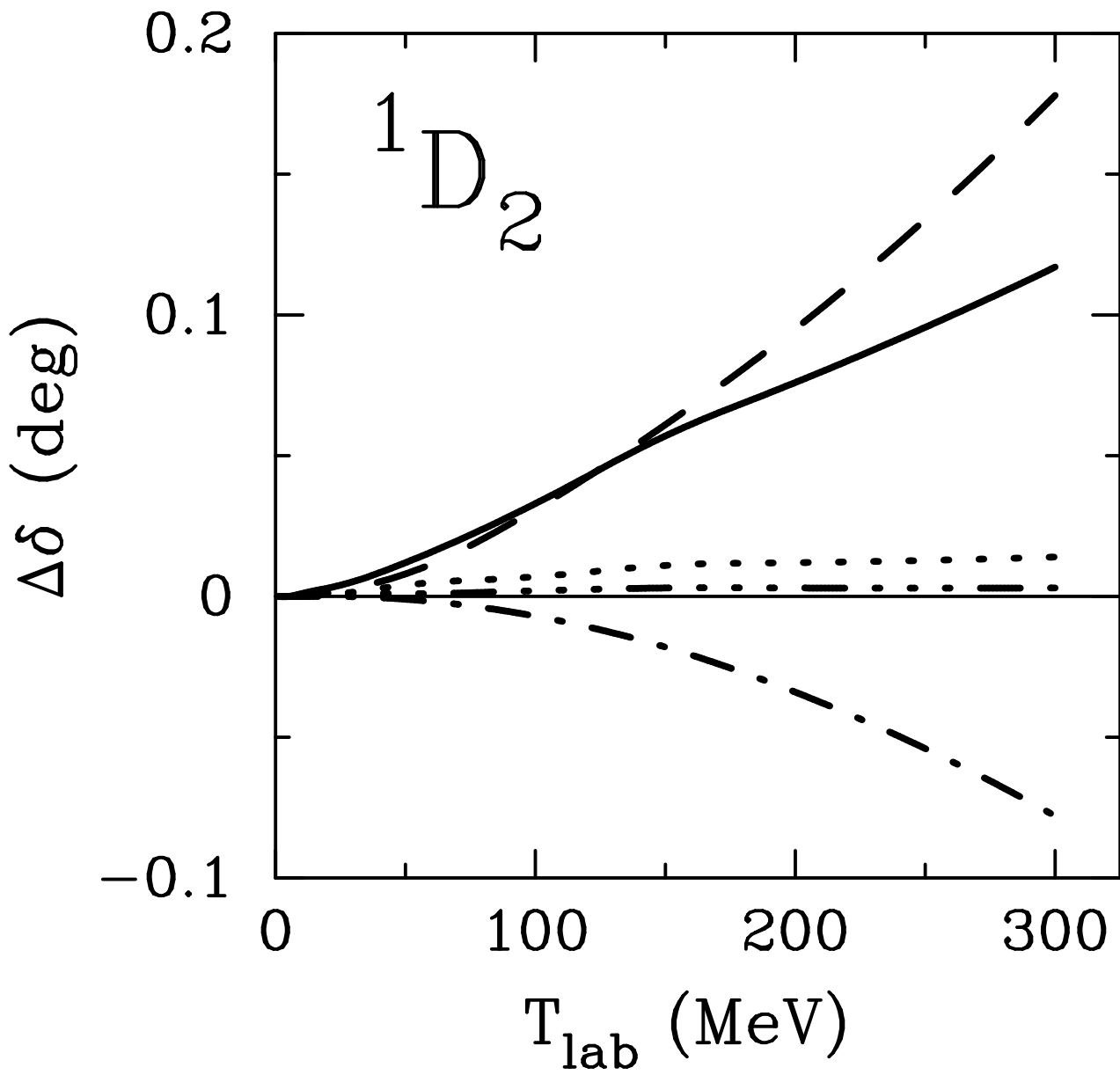
(b)

Li/Machleidt (CSB) Fig. 4

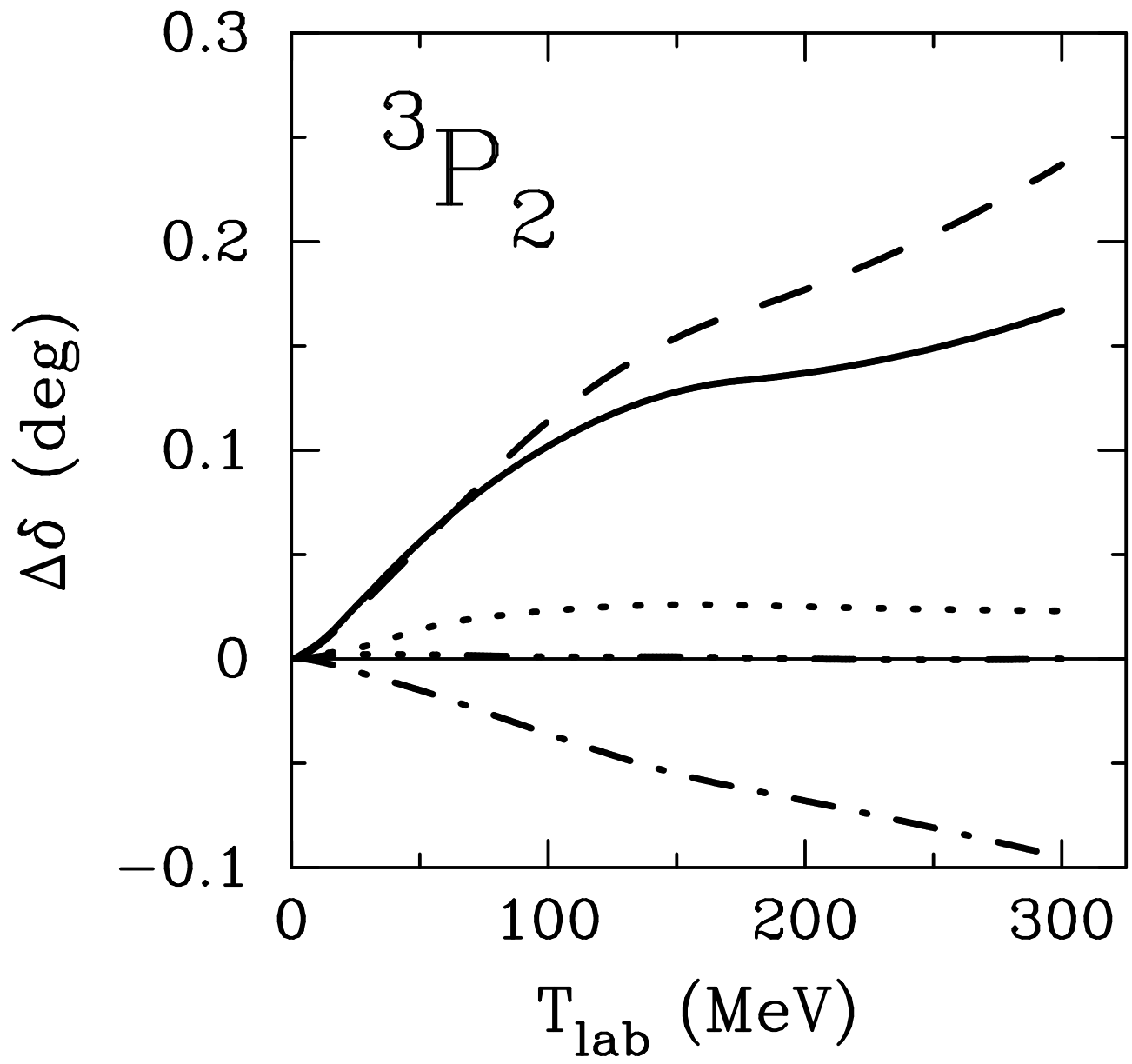


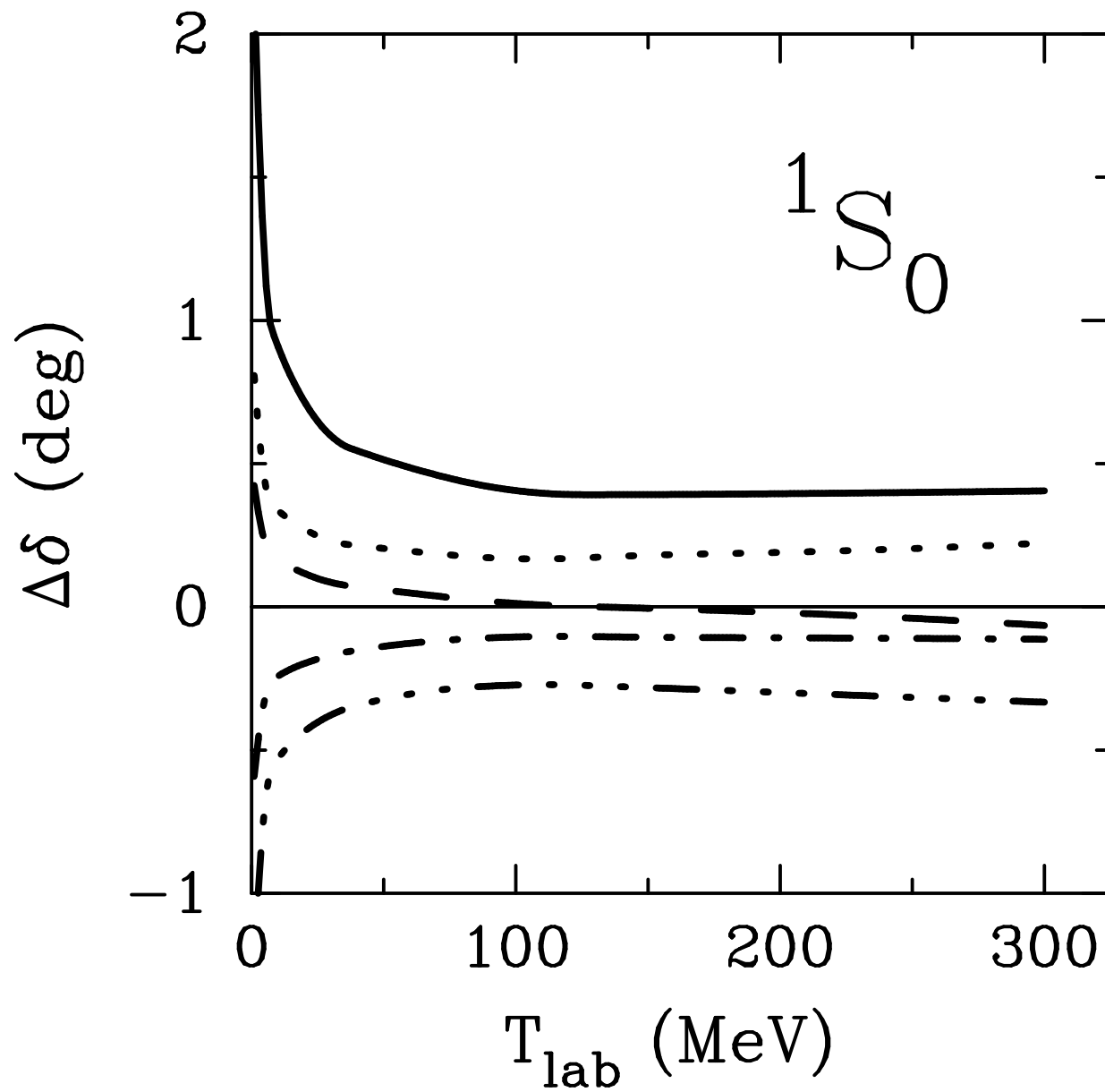


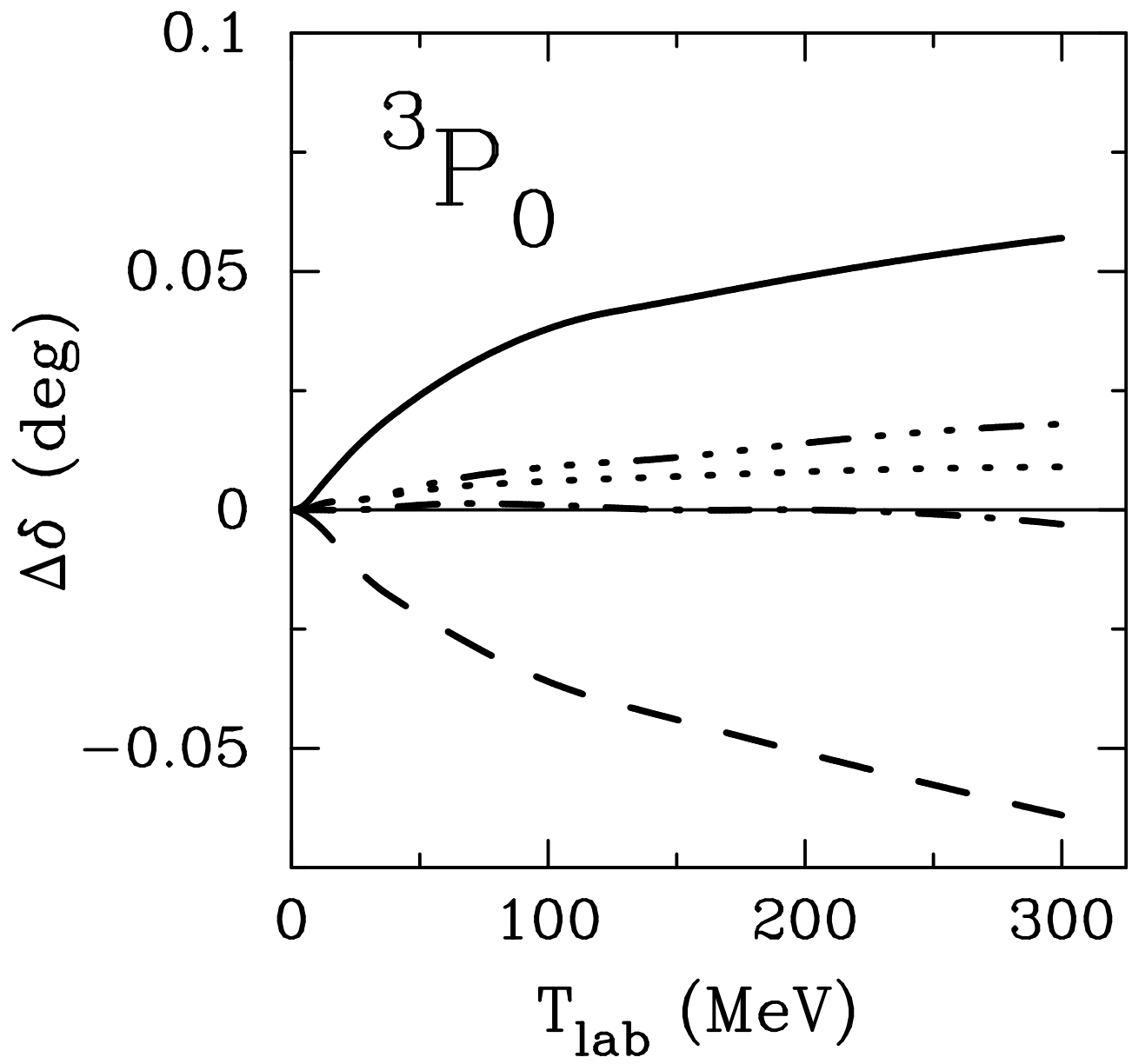


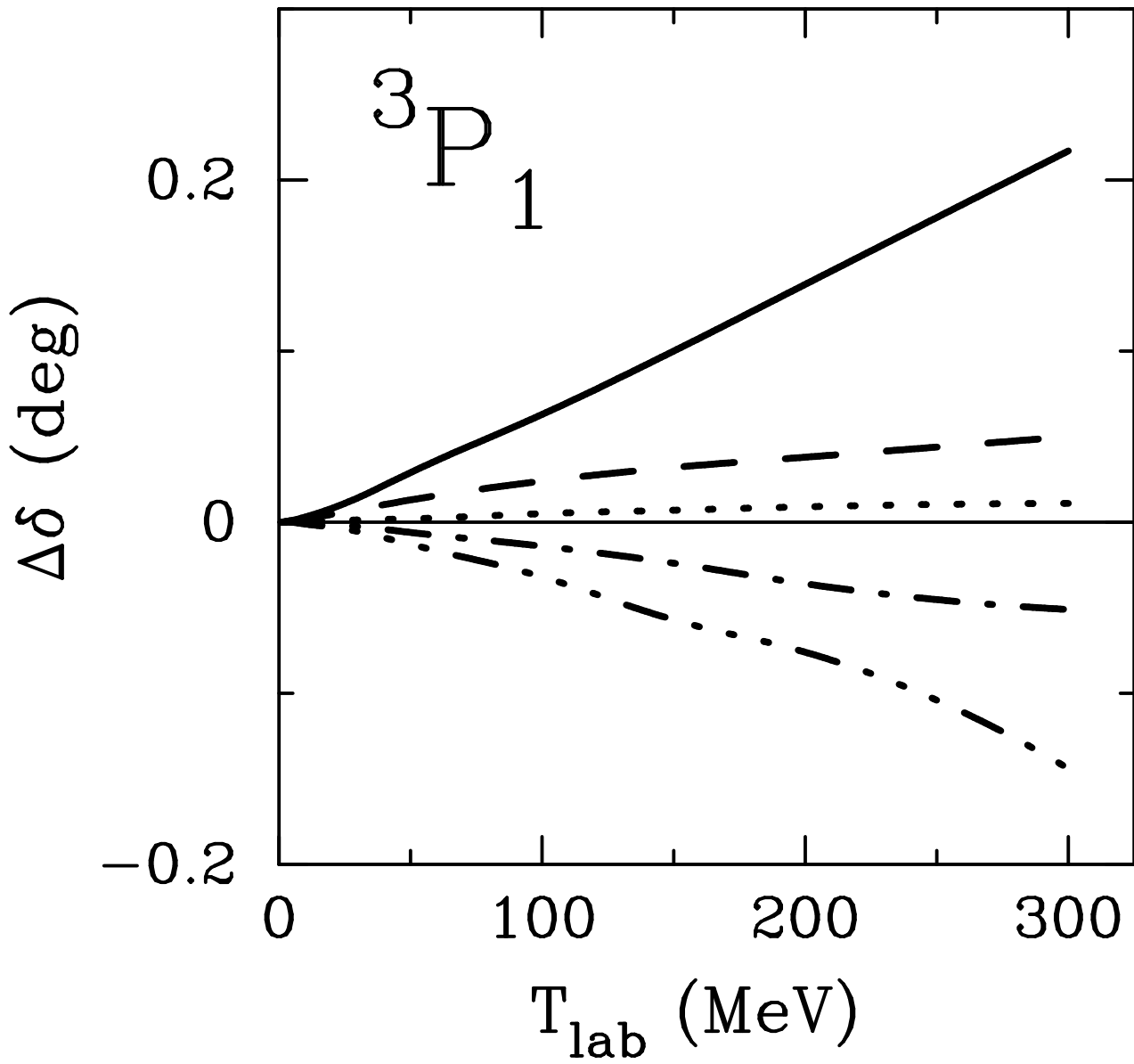


Li/Machleidt (CSB) Fig. 5, part 4 of 5









Li/Machleidt (CSB) Fig. 6, part 3 of 5

